Hindawi
Wireless Communications and Mobile Computing
Volume 2019, Article ID 4863823, 13 pages
https://doi.org/10.1155/2019/4863823

Research Article

Cooperative Closed-Loop Coded-MIMO Transmissions for Smart Grid Wireless Applications

Ndéye Bineta Sarr,[1,2] **Olufemi J. Oyedapo**,[3] **Basile L. Agba**,[4] **François Gagnon**,[1] **Hervé Boeglen**,[2] **and Rodolphe Vauzelle**[2]

[1] *École de Technologie Supérieure (ETS), Montréal, QC, Canada H3C 1K3*
[2] *XLIM Institute, University of Poitiers, 86360 Futuroscope, France*
[3] *McGill University, Montréal, QC, Canada*
[4] *Institut de Recherche d'Hydro-Québec (IREQ), Varennes, QC, Canada J3X 1S1*

Correspondence should be addressed to Ndéye Bineta Sarr; ndeye-bineta.sarr.1@ens.etsmtl.ca

Received 9 December 2018; Accepted 21 March 2019; Published 7 April 2019

Academic Editor: Laurie Cuthbert

Inherent interfering signals generated by the underlying elements found in power substations have been known to span over consecutive noise samples, resulting in bursty interfering noise samples. In the impulsive noise environments, we elaborate a space-sensitive technique using multiple-input multiple-output (MIMO), which is particularly well suited in these usually very difficult situations. We assume the availability of channel state information (CSI) at the transmitter to achieve typical MIMO system gains in ad hoc mode. In this paper, we show that more than 10 dB gains are obtained with the most efficient system that we propose for achieving smart grid application requirements. On the one hand, the results obviously illustrate that the max $- d_{min}$ precoder associated with the rank metric coding scheme is especially adapted to minimize the bit error rate (BER) when a maximum likelihood (ML) receiver is employed. On the other hand, it is shown that a novel node selection technique can reduce the required nodes transmission energies.

1. Introduction

Modernization of power grids is underway in many countries around the world. Induced by important factors such as national security, economic development, the environment, and the integration of renewable energies, the provinces, states, and countries are prioritizing technological innovations to be deployed to make the electricity network smarter: Smart Grid (SG). It consists of the integration of communication and information technologies into the networks and makes them communicate considering the actions of the players in the electricity system, while ensuring a more efficient, economically viable, and secure electricity supply. The aim is always to provide equity between supply and demand with increased responsiveness and reliability and to optimize network operations. In fact, such applications involve regular operations in real time, which require measurements from several sources. Recently, wireless sensor networks (WSN) have been identified as an encouraging technology to perform energy-efficient, seamless, reliable, remote monitoring, and low-cost control in SG applications [1]. Despite these benefits, WSN are facing some challenges including the dynamic topology, the unpredictable communication channel, and the limited power sources of nodes. In addition, in high-voltage (HV) substation environments, the inherent background additive white Gaussian noise (AWGN) is constantly present, but this classical observation is no longer relevant when the occurrence of an impulse becomes noticeable. In such realistic environments, noise signals generated by the underlying elements such as metallic structures (transformers, circuit breakers, disconnect switches, and transformers) span over several samples [2], giving rise to bursty appearances of impulses. To avoid the aforementioned constraints, the use of MIMO cooperative techniques [3–7] may be an obvious solution enabling nodes to be grouped into a set of virtual antennas as depicted in Figure 1.

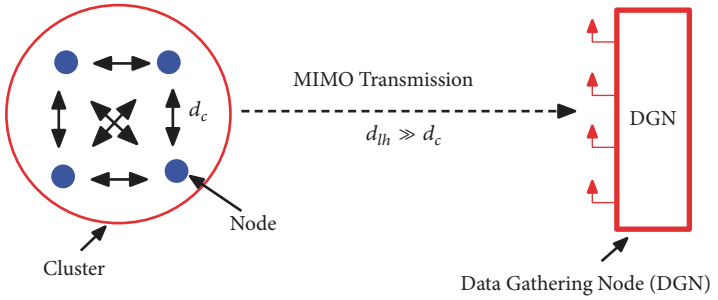

Figure 1: Cooperative MIMO system model.

Closed-loop cooperative transmission ensures that the source node cooperates with the idle neighbors to provide spatial diversity. Since the distance between nodes is smaller than the distance between the cluster and the data gathering node (DGN), each cooperating node then precodes the data before it transmits over the diverse subchannels to the receiver where data is combined and detected. Cooperative transmissions are well studied for improving the error rate probability or spectral efficiency performance. It has been shown that single input single output (SISO) and multihop approaches are less effective than cooperative transmission in terms of energy over long-haul distance [8]. By exploiting channel state information at the transmitter (CSI-T), a MIMO precoder can optimize specific criteria to increase system performance. The max – d_{min} precoder optimizes the Euclidean distance for improving the performance. The work in [7] highlighted the interest of using max – d_{min} by comparing the BERs and the mutual information with water filling (WF), lattice, and mercury water filling (MWF). The obtained results showed that the max – d_{min} achieved the best performance. Moreover, coded-MIMO ensures more efficiency and reliability in communication systems. For this purpose, it has also been largely studied for performance improvements. In [9, 10], the authors proposed a coded-MIMO based on Turbo codes and blockwise concatenated convolutional code (BCCC). The obtained results show significant improvements. Despite the encouraging results of these techniques, the weak points that are among others include the complexity of the decoding, the propagation of synchronization errors, and important time delays. In a previous study [11], we proposed a coded-orthogonal frequency division multiplexing (OFDM) system based on rank metric code (RC) and convolutional code (CC). The system approach was simple and robust for mitigating the bursty nature of impulsive noise occurring in the HV substations, even in a deterministic ray tracing channel. We had considered a deterministic channel extracted from a 3D ray tracing software called RapSor [12]. It is a 2D/3D ray tracing open and extensible tool which is associated with the uniform theory of diffraction (UTD) and the geometrical optic laws (GO). We now confirm that the same order of coding gain is maintained even with a closed-loop MIMO transmission. The objective of this paper is to provide a reliable and efficient communication system by combining the rank metric scheme and MIMO using a max – d_{min} precoder and reduce the energy transmission with an efficient node selection technique in an impulsive noise environment. The main contributions of this paper consist of the following.

(i) The max – d_{min} precoder approximation for binary phase shift keying (BPSK) modulation.

(ii) The proposition of a novel study case which takes into consideration the joint solution using an outer forward error correction (FEC) based on rank metric applied to the max – d_{min} MIMO precoder assuming maximum likelihood (ML) detection at the receiver.

(iii) The reduction of the complexity of our node selection technique assuming full channel state information (FCSI).

(iv) The reduction of the overall nodes transmission energy in bursty impulsive interferers.

The rest of the paper is presented as follows. Section 2 gives a review of impulsive noise models, particularly the Au model [13], while Section 3 considers the fundamentals of RC codes [14]. Section 4 presents the considered MIMO channel. Section 5 deals with the proposed system, the node selection technique, and cooperative MIMO. The obtained results are highlighted and discussed in Section 6. It first details the BER performance for the Rayleigh fading channel. Secondly, we assume that the channel is frequency-selective using RapSor. Section 7 is about the energy consumption model. Conclusion and outlook are provided in Section 8.

2. Review of Impulsive Noise Models

Impulsive noise is not only characteristic to substations; other environments like the industrial domains can introduce this noise and degrade communications as well. Several models of impulsive noise exist. They can be used depending on assumptions made in terms of the communication conditions. The popularly used models among others are Middleton Class A [15] and the Symmetric Alpha-Stable process [16]. However, the weak points of these models are that they do not take into consideration the correlation between successive pulses. Therefore, in recent years, two new models have been proposed in the literature. The first one is the partitioned Markov chain model (PMC-6) [17], and the second is the Au model [13], which will be discussed in this section. The PMC-6 model is a model with one state

representing the background noise considered as Gaussian and the 6 states are the impulse states. The transitions between several states are defined as a characterization of the remaining interaction between pulses. Nevertheless, due to the computational complexity of the model, we do not use it in this paper.

2.1. Au Noise. The "Au" noise model follows the physical concern of the mechanism making electromagnetic interference (EMI) in substations mostly generated by partial discharges (PD). Its model is considered as the first model that makes a link between the partial discharge evolution and the induced far-field oscillation propagation [13]. To characterize the PD, they proposed a process whose main components are the impulse detection composed of a denoising process, a short-time analysis, a detection, and a statistical analysis. Let us define $v(\mu, t)$ as the waveform of impulsive noise evaluated in volts per meter (V/m), such as μ is a total of random elements indicating its occurrence, duration, and other substantial characteristics. Considering $v_m(\mu, t)$ as the waveform quantified in V, one can represent

$$v(\mu, t) = v_m(\mu, t) \sqrt{\frac{Z_0 4\pi}{L_r G_{rf} \lambda^2}} \tag{1}$$

where L_r represents the load resistance and G_{rf} the RF system gain, while λ corresponds to the wideband antenna wavelength, and $Z_0 = 120\pi\Omega$ is the free-space impedance. In practice, the final noise received by an antenna can be indicated as follows:

$$x(\mu, t) = \sum_k v_k(\mu, t) + B_n(t) \tag{2}$$

where $B_n(t)$ is the background noise generally considered as Gaussian. During a long observation period, the resultant signal is formed by a superposition of several transient impulse waveforms. For a better location of the impulse, a denoising process is used. It consists of extracting the pulses from the noise. This operation is done using a wavelet transformation to which a threshold, namely, $C_r = s^2\sqrt{2\log(K_i)}$ is exercised. K_i is the sample at the moment i, and s^2 is the variance of the background Gaussian noise. The data obtained from measurements are made up of a sequence of pulses located arbitrarily in time. Partial discharges can be identified applying a temporal interpretation of the waveform spectrogram $V(\mu, t_g, f)$ given by

$$V(\mu, t_g, f) = \int v(\mu, t)\, g(t - t_g)\, e^{-j2\pi f t} dt \tag{3}$$

such that $g(t)$, whose length is t_g, is a quadratically integrable temporal window function. The Au model has been compared to measurements from different levels of voltage such as 25, 230, 315, and 735 kV electrical substations. The setup of measurement used is well described in [13, 17]. To validate its model, a comparison between experimentation and simulation results was produced in [18], which shows that the Au model is the best model to represent impulsive noise in substations.

3. Principles of Rank Metric Coding Scheme

Introduced by Delsarte in coding theory [14] and developed by E. Gabidulin [19], the RC or Gabidulin codes are widely employed in cryptography. However, recently, it has been introduced in communication systems to improve the performance degraded by noise such as impulsive noise represented as a matrix in a row or column. In [11, 20], the authors used RC concatenated with a CC in their systems. Their results showed that with these codes, it is possible to mitigate the impulsive noise occurring in industrial environments such as power substations.

Considering the significant improvements and the low complexity of these codes compared to the traditional Turbo codes and Reed-Solomon (RS) codes [20], we use this coding scheme in our system. For this purpose, we start with the definition of some meaningful parameters of this coding scheme.

Let q be a power of a prime and $\mathbb{F}_q$ designate Galois Field with q elements. Let $\mathbb{F}_q^{v\times u}$ express the $v \times u$ matrices over $\mathbb{F}_q$, and set $\mathbb{F}_q^v = \mathbb{F}_q^{v\times 1}$. Let $\mathbb{F}_q^u$ be an extension of $\mathbb{F}_q$. Every extension field can be considered as a vector space over the finite field. Let $\mathscr{B} = \beta_0, \beta_1, \cdots, \beta_{u-1}$ be a basis for $\mathbb{F}_q^u$ over $\mathbb{F}_q$. Since $\mathbb{F}_q^u$ is also a field, we may consider a vector $\in \mathbb{F}_q^u$. Whenever $\in \mathbb{F}_{q^u}^v$, we denote by x_i the i^{th} entry of x; that is, $x = [x_0, x_1, \ldots, x_{v-1}]^T$. It is natural to extend the map $[\bullet]$ to a bijection from $\mathbb{F}_{q^u}^v$ to $\mathbb{F}_q^{v\times u}$, such that the i^{th}row of $[x]_{\mathscr{B}}$ is expressed by $[x_i]_{\mathscr{B}}$.

RC codes are described as a nonempty subset $\mathscr{X} \subseteq \mathbb{F}_q^{v\times u}$. The rank weight of x, defined as $\mathscr{R}k(x)$, is denoted to be the maximum number of coordinates in x that are linearly independent over $\mathbb{F}_q$.

The *rank distance* between two vectors x_1 and x_2 is the column rank of their difference $\mathscr{R}k(x_1 - x_2 \mid \mathbb{F}_q)$. The rank distance of a vector rank code $\mathscr{X} \subset \mathbb{F}_{q^u}^v$ is expressed as the *minimal rank distance*:

$$d(\mathscr{X}) = d = \min\left(\mathscr{R}k\left(x_i - x_j\right) : x_i, x_j \in \mathscr{X},\ i \neq j\right) \tag{4}$$

For $u \geq v$, an important class of rank metric codes was proposed by Gabidulin [21]. Gabidulin code is a linear (v, k, d) block code over $\mathbb{F}_{q^u}$ defined by the parity-check matrix $P = [p_j^{[i]}]; 0 \leq i \leq v - k - 1,\ 0 \leq j \leq v - 1$, where the elements $(p_0, p_1, \ldots, p_{v-1}) \in \mathbb{F}_{q^u}$ are linearly independent over $\mathbb{F}_q$ and $k = v - d - 1$ is the dimension of the code. The parity matrix defines a maximum rank distance (MRD) code with length $v \leq u$ and $d = v - k + 1$. Another method for MRD construction can be obtained using generator matrices [21].

For rank error correction, we consider a MRD (v, k, d) code $\mathscr{X}$. The transmitted signal is x and received signal can be depicted as $y = x + e_{eff}$, such that e_{eff} is an error. Vector errors that can be corrected by the code $\mathscr{X}$ are of the form

$$e_{eff} = e + e_{row} + e_{col} \tag{5}$$

where e, e_{row}, and e_{col} are a random rank error of rank t, a vector rank row erasure, and a vector rank column erasure,

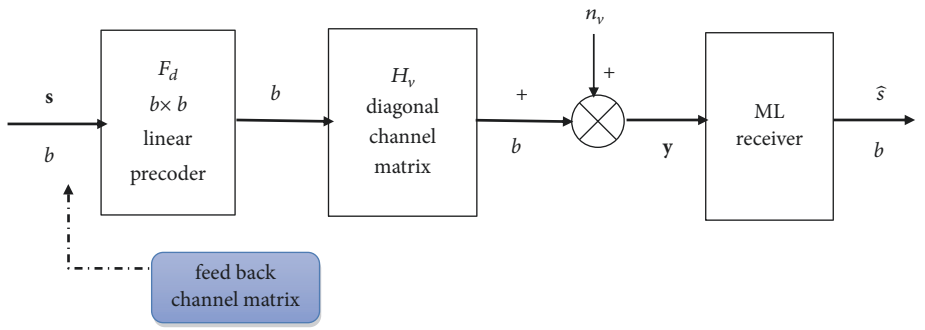

Figure 2: Equivalent MIMO system with a linear precoder in virtual channel.

respectively. Fast correction of rank erasures and random rank errors was presented in [19]. It is called the modified Berlekamp-Massey algorithm. For more information, readers are referred to [21, 22]. This is an effective technique for decoding RC errors and will be used in this paper.

4. Closed-Loop MIMO

For a MIMO channel with no delay spread, comprising F and G, which are the precoder and decoder matrices, respectively, the following linear system equation applies:

$$\mathbf{y} = \mathbf{GHFs} + \mathbf{Gn} \tag{6}$$

such that s is the $b \times 1$ transmitted symbol vector, y is the $b \times 1$ received vector, n is an $n_r \times 1$ additive noise vector, H is the channel matrix of $n_r \times n_t$; here, n_r and n_t are the numbers of the receive and transmit antennas, respectively, and $\mathbf{F}$ is the $n_t \times b$ precoder matrix. We suppose that $b \leq rank(\mathbf{H}) \leq \min(n_t, n_r)$ and

$$\begin{aligned} \mathbb{E}\{ss^*\} &= \mathbf{I_b}, \\ \mathbb{E}\{nn^*\} &= N_0\mathbf{I_b} \end{aligned} \tag{7}$$

The FCSI permits the precoder to diagonalize the channel into b parallel SISO channels as depicted in Figure 2. If E_T is the total available power, the following power constraint is applied to the transmitter:

$$\text{trace}\left[\mathbf{FF}^*\right] = E_T \tag{8}$$

The precoding and decoding matrices are separated into two components as $\mathbf{F} = \mathbf{F_v}\mathbf{F}_d$ and $\mathbf{G} = \mathbf{G}_v\mathbf{G}_d$, respectively. The unitary matrices, $\mathbf{G}_v$ and $\mathbf{F}_v$, derived from the singular value decomposition (SVD) of $\mathbf{H}$, diagonalize the channel and decrease the scope to 2. Hence, the received symbol in (6) becomes

$$\mathbf{y} = \mathbf{G}_d\mathbf{F}_d\mathbf{H}_v\mathbf{s} + \mathbf{G}_d\mathbf{n}_v \tag{9}$$

such that $\mathbf{H}_v = \mathbf{G}_v\mathbf{HF}_v = \text{diag}(\beta_1, \beta_2, \ldots, \beta_b)$ is the virtual channel matrix, β_i denote the gains of the subchannel sorted in decreasing structure, and $\mathbf{n}_v = \mathbf{G}_v\mathbf{n}$ is the $b \times 1$ channel virtual noise. Since the ML detection will be used in the following sections, the decoding matrix $\mathbf{G}_d$ does not influence the efficiency and is considered to be $\mathbf{I_b}$.

4.1. Minimum Euclidean Distance Precoding: $\max - d_{min}$. The precoder $\max - d_{min}$ consists of the maximization of the minimum Euclidean distance d_{min} between the signal items at the receiver as

$$d_{min}(\mathbf{F}_d) = \min_{(s_{k-s_l}),k\neq l} \left\|\mathbf{H}_v\mathbf{F}_d(\mathrm{s_k} - \mathrm{s_l})\right\| \tag{10}$$

Let us define $\mathbf{e} = (\mathbf{s_k} - \mathbf{s_l})$ as the difference between possible transmitted vectors. Thus, $d_{min}(\mathbf{F}_d)$ becomes

$$d_{min}(\mathbf{F}_d) = \min_e \left\|\mathbf{H}_v\mathbf{F}_d\mathbf{e}\right\| \tag{11}$$

Therefore, its optimization problem entails finding the matrix F_d, which maximizes the criterion

$$\begin{aligned} \mathbf{F}_d^{d_{min}} &= \underset{\mathbf{F}_d}{\text{argmax}} \left\{d_{min}(\mathbf{F}_d)\right\} \\ &= \underset{\mathbf{F}_d}{\text{argmax}} \left\{\min_e \left\|\mathbf{H}_v\mathbf{F}_d\mathbf{e}\right\|\right\} \end{aligned} \tag{12}$$

Since the ML detection will be considered, this criterion is well suited because the probability of symbol errors relies on the minimum Euclidean distance.

However, determining the solution of $\mathbf{F}_d$ is complicated due to the large solutions space and the alphabet symbols which it processes. For this purpose, we propose to simplify the technique and derive a solution for b = 2 virtual channels. Hence, the channel virtual matrix can be expressed as

$$\mathbf{H}_v = \begin{pmatrix} \sqrt{\beta_1} & 0 \\ 0 & \sqrt{\beta_2} \end{pmatrix} = \sqrt{2\beta}\begin{pmatrix} \cos\alpha & 0 \\ 0 & \sin\alpha \end{pmatrix} \tag{13}$$

where α is the channel angle and $\alpha \in [0, \pi/4]$ and $\beta = (\beta_1 + \beta_2)/2$. This solution does not rely on the SNR, but is based on the channel angle α.

The SVD applied to the matrix precoder is as follows:

$$\mathbf{F}_d = \mathbf{Q}\sum\mathbf{R}^* \tag{14}$$

where $\sum$ is the diagonal matrix and Q and R are $b \times b$ unitary matrices.

Recall that the power constraint at the transmit antennas always remains; $\sum$ must fulfill the constraint too and is derived as

$$\sum = \sqrt{E_T}\begin{pmatrix} \cos\gamma & 0 \\ 0 & \sin\gamma \end{pmatrix} \tag{15}$$

with $0 \leq \gamma \leq \pi/4$.

Since the matrix $\mathbf{R}^*$ has no influence on the singular values, they can be derived from $\mathbf{H}_v\mathbf{Q}\sum$. The largest singular values are obtained when $Q = I_2$.

Proof of $\mathbf{Q} = \mathbf{I_2}$. Consider the form of the unitary matrix of Q

$$\mathbf{Q} = \begin{pmatrix} (\cos\theta)\, e^{i\theta_1} & (\sin\theta)\, e^{i\theta_3} \\ -(\sin\theta)\, e^{i\theta_2} & (\cos\theta)\, e^{i\theta_4} \end{pmatrix} \tag{16}$$

with the constraints

$$(\theta_1 + \theta_4) = (\theta_2 + \theta_3) \mod 2\pi \tag{17}$$

The angle $\theta \in 0 \le \theta < \pi/2$.

Recall that the single values are null or (positive and real), and the determinant of a unitary matrix = 1. We define $\mathbf{U} \wedge \mathbf{V}^*$ as the single value decomposition of $\mathbf{H}_v\mathbf{Q}\sum$ and σ_k, the diagonal components of $\wedge$. The product of SV is not based on Q. In fact, we can note that

$$\begin{aligned} \sigma_1\sigma_2 &= \left|\det\left(\bigwedge\right)\right| = \left|\det\left(\mathbf{U} \wedge \mathbf{V}^*\right)\right| = \left|\det\left(\mathbf{H}_v\mathbf{Q}\sum\right)\right| \\ &= \left|\sqrt{(\beta_1\beta_2)}E_T \cos\gamma \sin\gamma \det(\mathrm{Q})\right| \\ &= \sqrt{(\beta_1\beta_2)}E_T \cos\gamma \sin\gamma \end{aligned} \tag{18}$$

Moreover, we have

$$\begin{aligned} {\sigma_1}^2 + {\sigma_2}^2 &= \mathrm{trace}\left(\wedge^2\right) = \mathrm{trace}\left(\mathrm{U} \wedge \mathrm{V}^*\mathrm{V} \wedge \mathrm{U}^*\right) \\ &= \left\|\mathbf{U} \wedge \mathbf{V}^*\right\|_{\mathrm{F}}^2 = \left\|\mathbf{H}_v\mathrm{Q}\sum\right\|_{\mathrm{F}}^2 \end{aligned} \tag{19}$$

Therefore, the phases of the constituents of Q do no impact on ${\sigma_1}^2 + {\sigma_2}^2$. Eventually, we deduce that the single values do not rely on the phases of the constituents of Q. Thus, we just assume real matrices Q, whose typical structure is

$$\mathrm{Q} = \begin{pmatrix} \cos\theta & \sin\theta \\ -\sin\theta & \cos\theta \end{pmatrix} \tag{20}$$

where $0 \le \theta < \pi/2$.

We now examine the sum of the square single value of $\mathbf{H}_v\mathbf{Q}\sum$.

$$\begin{aligned} {\sigma_1}^2 + {\sigma_2}^2 &= \left\|\mathbf{H}_v\mathbf{Q}\sum\right\|_{\mathrm{F}}^2 = \mathrm{trace}\left(\mathbf{H}_v\mathbf{Q}\sum\sum\mathbf{Q}^*\mathbf{H}_v\right) \\ &= E_T(\beta_1 \sin^2\gamma + \beta_2 \cos^2\gamma \\ &\quad + (\beta_1 - \beta_2)\cos(2\gamma)\cos^2\theta \end{aligned} \tag{21}$$

As $\beta_1 > \beta_2$, for every σ_1, the maximum value of σ_2 is acquired for $\theta = 0$, which is denoted as $Q = I_2$. □

Hence, $\mathbf{R}^*$ can be simplified as follows:

$$\mathbf{R}^* = \begin{pmatrix} \cos\varpi & (\sin\varpi)\, e^{i\varphi} \\ -\sin\varpi & (\cos\varpi)\, e^{i\varphi} \end{pmatrix} \tag{22}$$

while developing

$$\mathbf{R}^* = \begin{pmatrix} \cos\varpi & \sin\varpi \\ -\sin\varpi & \cos\varpi \end{pmatrix} \begin{pmatrix} 1 & 0 \\ 0 & e^{i\varphi} \end{pmatrix} = \mathrm{R}_{\varpi}\mathrm{R}_{\varphi} \tag{23}$$

with $0 \le \varphi < 2\pi$ and $0 \le \varpi \le \pi/2$.

Thus, the precoder can be expressed as

$$\mathbf{F}_d = \sqrt{E_T} \begin{pmatrix} \cos\gamma & 0 \\ 0 & \sin\gamma \end{pmatrix} \begin{pmatrix} \cos\varpi & \sin\varpi \\ -\sin\varpi & \cos\varpi \end{pmatrix} \begin{pmatrix} 1 & 0 \\ 0 & e^{i\varphi} \end{pmatrix} \tag{24}$$

4.2. Solution for BPSK Modulation. Considering a Binary Phase Shift Keying (BPSK) technique, where $b = 2$, the data symbols are in $\{1, -1\}$ and the difference vectors related to $\mathbf{e} = (\mathbf{s_k} - \mathbf{s_l})$ are $\left\{\binom{0}{2}, \binom{0}{-2}, \binom{2}{0}, \binom{2}{2}, \binom{2}{-2}, \binom{-2}{0}, \binom{-2}{2}, \binom{-2}{-2}\right\}$. Since some vectors are collinear, the solution is reduced $\mathbf{e_{BPSK}} = \left\{\binom{0}{2}, \binom{2}{0}, \binom{2}{2}, \binom{-2}{-2}\right\}$. A numerical search over γ, ϖ, and φ which maximizes the smallest distance for difference vectors in $\mathbf{e_{BPSK}}$ demonstrates that whatever the channel, i.e., whatever the channel angle α, the precoder which maximizes d_{min} is obtained for $\gamma = 0^\circ$, $\varpi = 45^\circ$, and $\varphi = 90^\circ$.

Hence, by substituting for the real values, we can deduce the solution for BPSK modulation, which is given as follows:

$$\mathbf{F}_d\,(BPSK) = \mathbf{F}_{BPSK} = \sqrt{\frac{E_T}{2}} \begin{pmatrix} 1 & \sqrt{-1} \\ 0 & 0 \end{pmatrix} \tag{25}$$

And its d_{min}, namely, d_{min}^{BPSK}, is

$$d_{min}^{BPSK} = \left\|\mathbf{H}_v\mathbf{F}_{BPSK} \begin{pmatrix} 2 \\ 0 \end{pmatrix}\right\| = 2\sqrt{\beta E_T}\cos\alpha \tag{26}$$

Notice that the second row of (25) is equal to 0, indicating that the signal is completely transmitted on the most favored subchannel. This solution could be compared to the max SNR that streams power just on the strongest eigenmode of the channel [23].

The distance (26) normalized by $\sqrt{2\beta E_T}$ is depicted in Figure 3 [24], showing that this distance depends on the channel angle.

5. System Model and Cooperative MIMO

5.1. Description. The system model which is considered in this paper is depicted in Figure 1. We assume transmissions from a cluster of n_c nodes to the DGN over Rayleigh fading channels and a realistic channel model obtained with the RapSor simulator. Any node $i (i = 1, 2, \ldots, n_c)$ in a cluster k is a single-antenna node with the capability to be a slave or a cluster-head. A node acting as a cluster head synchronizes its $n_c - 1$ neighbors, while a slave cooperates with other nodes in cluster k over a relatively short SISO communication link. The DGN is a multiantenna receiver and equipped with relatively high processing capabilities and without energy constraints. Assume this scenario, where substation elements and infrastructure are fitted with several wireless sensors such as temperature, pressure, and electrical parameters (voltage,

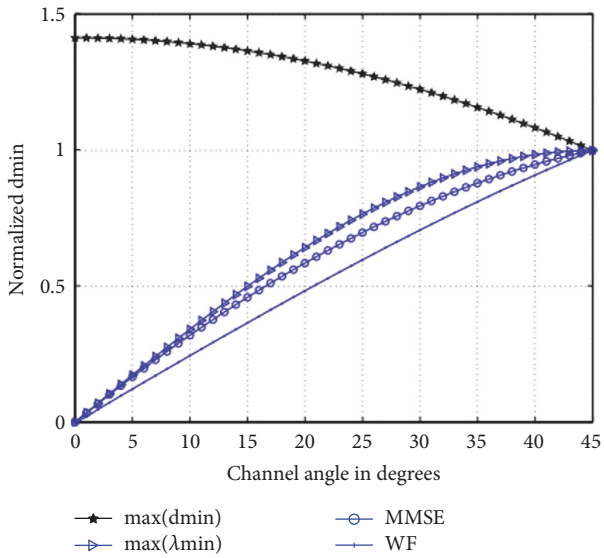

Figure 3: Normalized Euclidean distance for BPSK modulation.

current, and frequency). Such sensor nodes are required to measure and cooperatively transmit measured data wirelessly to DGN over a distance d_{lh}. Due to relatively shorter distances dc between cooperating nodes, an AWGN channel is assumed with no fading, while Rayleigh fading is supposed to be fixed overall the transmission of the codeword from the cluster to the DGN over the distance d_{lh}. The communication protocol depicted in Figure 4 can be described as follows.

(i) *Declaration Phase*. We assume neighborhood discovery had been previously performed. Any source node having data to transmit forms a cluster and confirms itself as the cluster head since the first which declares is considered as the head of the cluster. All the nodes which "hear" the source node set their "status" to slave ready to receive from the source. In an event that two or more nodes perform declaration, the cluster-head with the least residual energy Eres wins, but nodes with data can still send to neighboring nodes after the current cluster-head.

(ii) *Phase 1*. The source node multicasts its data to $n_c - 1$ neighbors over the average distance of dc; this is a SISO communication.

(iii) *Phase 2*. Next, the $n_c - 1$ neighbors, as potential relays, send each training frame *tra*. to the DGN which uses this to estimate the multipath coefficients for each of its received antennas. The DGN also notes the identification (ID) of the cluster-head for future acknowledgment. It then constructs the channel matrix H and selects the best n_t nodes, including the optimal precoding matrix index for the selected nodes.

(iv) *Phase 3*. The DGN selects n_t nodes that will use the precoding matrix whose index is found in the precoding message *prec*. sent by the DGN to n_t nodes. The message *prec*. also includes the ID of the selected nodes.

(v) *Phase 4*. The n_t selected nodes precode with the precoding matrix and then transmit the data frames to the DGN using MIMO transmission over a Rayleigh channel or a channel obtained with RapSor.

5.2. Cooperative MIMO. When the FCSI is available, $\mathbf{F}_v$ is a unitary matrix derived from SVD of the channel matrix H. In practical applications, the hypothesis of FCSI availability at the transmitter is unrealistic; rather the channel information must be made available to the transmitter from the receiver via the rate-limited feedback control channel [25]. The channel information types that can be made available include the channel statistics, instantaneous channel, and partial or quantized CSI (QCSI). The most practical of these is the QCSI because the feedback amount can be adjusted to the available rate of the feedback control channel. In the case of the limited CSI, we implement a finite codebook in which the receiver selects the optimal matrix $\mathbf{F}_d$ and $\mathbf{F}_v$ from $\mathcal{F}_v$ and $\mathcal{F}_d$ dictionaries. The optimal dictionary $\mathcal{F}_v$ containing a set $\{F_{v1}, F_{v2}, \ldots, F_{vN}\}$ is implemented according to the algorithm in [26], where $N = 2^{B_1}$ is the dictionary size, and B_1 is the number of quantization bits. Generally, constructing the $\mathcal{F}_d$ dictionary is required for each H realization in conjunction with the F_v dictionary, but for the BPSK modulation, the content of dictionary $\mathcal{F}_d$ will be limited to a single precoder matrix F_d since it is independent of the channel angle. The two dictionaries are generated offline, combined into a codebook $\mathcal{F} = \mathcal{F}_v\mathcal{F}_d = (F_{v1}, F_{v2}, \ldots, F_N)$, and are made available to all nodes. The codebooks for 2, 3, and 4 transmit nodes are generated with 3, 5, and 7 bits resolution, respectively, and are used for all our simulations.

5.3. Nodes Selection. Node selection is performed by the DGN to select n_t nodes from a cluster of interest by d_{min} associated with each node as

$$d_{min}\left(h^{(j)}\right) = \min_{e'} \left\| \mathbf{G}_v^{(j)} \mathbf{h}^{(j)} \mathbf{F}^{(j)} \mathbf{e}' \right\| \tag{27}$$

where $\mathbf{G}_v^{(j)}[1 \times n_r]$, $h^{(j)}$ is the j^{th} column of the cluster destination channel matrix $\overline{\mathbf{H}}[n_r \times n_t]$, $F^{(j)}$ is the associated precoding matrix j^{th} column of $\overline{\mathbf{H}}$, and e' is the difference between possible transmitted vectors belonging to a set $\{-1; 1\}$. Due to constraint $b \leq \min(n_r, n_t)$, $\mathbf{F}_d^{(j)}$ becomes a scalar. The unitary matrix $\mathbf{F}_v^{(j)}$ obtained by the method of dictionary construction explained previously (or by SVD for FCSI) is a scalar, i.e., $\mathbf{F}_d^{(j)} = \mathbf{F}_v^{(j)} = 1\mathrm{F(j)}$. Sorted in descending order, the n_t indexes of the eigenvalues corresponding to the column vectors of matrix $\overline{\mathbf{H}}$ are the n_t columns of matrix H of selected nodes. Nodes can be selected faster as opposed maximizing the d_{min} of L subcarriers for each $\overline{\mathbf{H}}$, where $\mathrm{L} = n_c!/n_t(n_c - n_t)!$.

6. BER Performance Analysis

This section introduces numerical results performed by simulations under Rayleigh and RapSor channels affected by Gaussian noise and Au impulsive noise. We assume ML

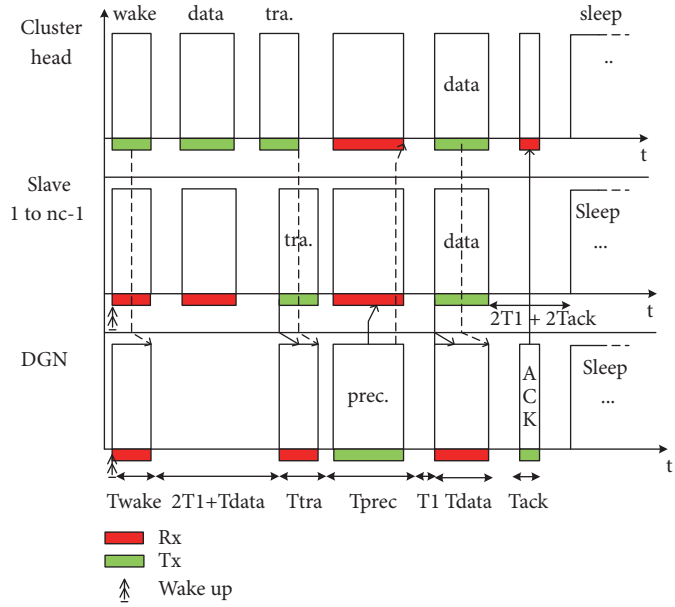

Figure 4: The assumed cooperative protocol.

detection at the DGN; indeed, the average probability of error limited to the nearest d_{min} neighbors [27] can be approximated as

$$P_e \approx \frac{\overline{N}_n}{2}\left(\sqrt{\frac{(d_{min})^2 E_T}{4\sigma^2}}\right) \quad (28)$$

such that $\overline{N}_n$ is the mean of the nearest neighbors. Considering a BPSK modulation, the bit error probability is given by

$$P_{bit} \approx \frac{\overline{N}_n}{2b\log_2 M}\operatorname{erfc}\left(\sqrt{\frac{\left(d_{min}^{BPSK}\right)^2 E_T}{4\sigma^2}}\right) \quad (29)$$

where M = 2 is the modulation order and erfc is the complementary error function. To estimate the performance of MIMO system with max − d_{min} precoder, the MATLAB software is utilized. The simulation started with uncoded MIMO system and then used concatenated RC/CC in the presence of Gaussian noise and Au impulsive noise. Two configurations are also considered: a transmission without node selection and a transmission with node selection. MIMO system efficiency is investigated for both Rayleigh fading and RapSor channels. The reliability of the system is expressed by the correlation between bit error rate (BER) versus the signal to noise ratio (SNR). Firstly, the system described with no channel coding approaches is to demonstrate the impact of employing coding scheme in cooperative MIMO system by utilizing BPSK modulation over AWGN and impulsive noise with Rayleigh fading and RapSor channels. We also investigated the performance of concatenated RC and CC. The size of Galois Field for the RC is $\mathbb{F}_{q^u} = 16$, while the CC employed has a coding rate $R = 1/2$ and generator polynomials in octal form: $P_1 = 171$ and $P_2 = 133$. The decoding of RC is implemented by the modified Berlekamp-Massey, while CC decoding is performed by soft decision of Viterbi algorithm.

6.1. AWGN and Impulsive Noise under Rayleigh Channel

6.1.1. Transmission without Node Selection. Figure 5 depicts BER performance of max − d_{min} MIMO precoding with FCSI without node selection. The results demonstrate that the worst performance of MIMO system is with no channel coding for both AWGN and impulsive noise. Uncoded-MIMO indicates a flattening of the BER between -5 and 5 dB. Then, it is improved by adding coding technique. Using concatenated RC/CC with max − d_{min} precoding in MIMO system gives more improvement to the system. Considering the presence of impulsive noise, the coding gain between uncoded and suggested approach is approximately 8 dB at a target BER of 10^{-4}. We now compare our results to those obtained in [28]. The authors proposed an effective technique to track the double-selected multipath channel for MIMO-OFDM system. A Space Time Block Coding (STBC) is applied and leads to interesting performance. However, our system is more robust and presents better performance. We have a gain of approximately 12 dB compared to the proposed approach described above. Furthermore, in [29], the authors presented a MIMO-OFDM system with a concatenated RS/CC. The system is evaluated in both Rayleigh and Rician channels. The obtained results are improved compared to an uncoded system. However, our system still has the best performance.

6.1.2. Transmission with Node Selection. The first simulations we made concerned the transmission without node selection. In this paragraph, we present numerical results when optimal and suboptimal node selection are implemented combined with the knowledge of the channel (FCSI or QCSI). Assuming

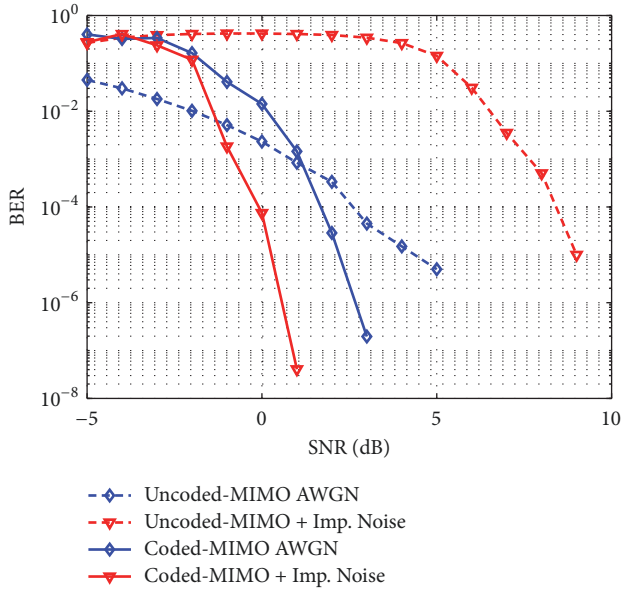

FIGURE 5: BER performance of max – d_{min} MIMO precoding with FCSI under Rayleigh channel without node selection.

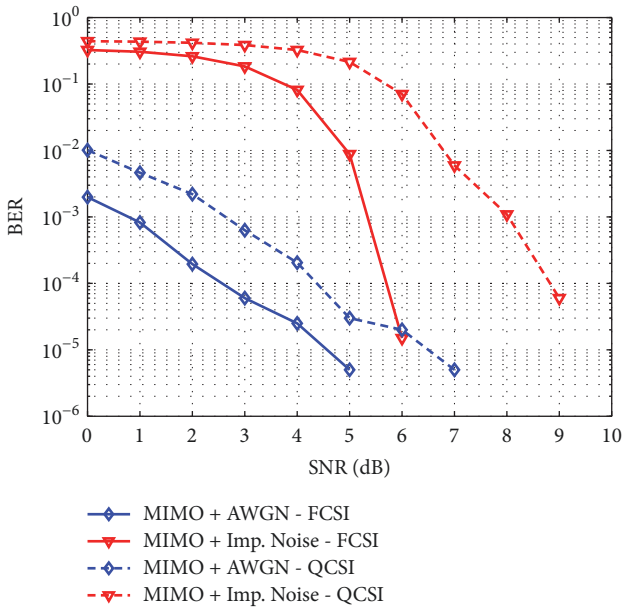

FIGURE 6: Performance comparison between FCSI and QCSI: curves with solid lines represent FCSI, while dashed lines represent the QCSI.

the full channel knowledge, the system model described in Section 4 is implemented. For the QCSI, a codebook quantized using 3, 5, and 7 bits for 2, 3, and 4 selected nodes is considered, respectively. The performances are shown in Figures 6 and 7. Results are only shown for 4 transmit nodes. In Figure 5, the results of uncoded systems are presented, and the performances between FCSI and QCSI are compared. As can be seen, FCSI outperforms QCSI for both AWGN and impulsive noise. Since FCSI yields better performance results than QCSI, we represent only results in FCSI with the

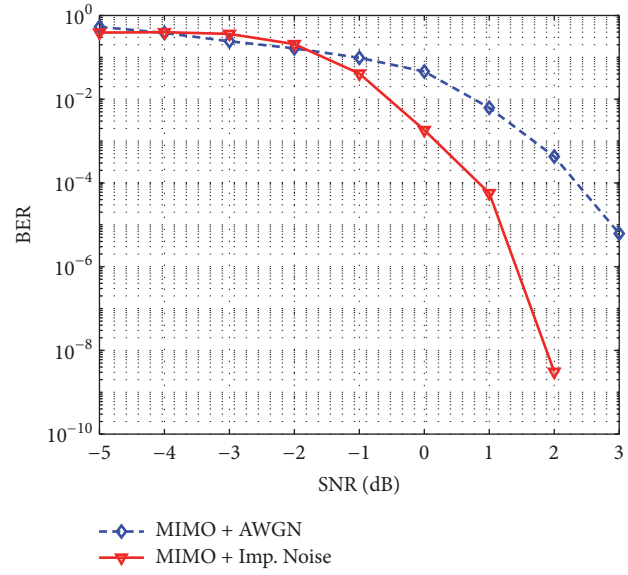

FIGURE 7: Coded-BER performance of max – d_{min} precoding under Rayleigh fading channel with FCSI and node selection.

node selection in Figure 7, which shows simulation results with a coded system. As for the case without selection, a performance improvement can be noticed. Considering a channel impaired by impulsive noise and a concatenated RC/CC, a target BER of 10^{-4} is achieved at an SNR of approximately 1 dB. It leads to a coding gain of 4.7 dB between uncoded and coded MIMO systems.

6.2. AWGN and Impulsive Noise under a RapSor Channel. In the preceding section, we studied the impact of coded-MIMO communications under a Rayleigh fading channel affected by impulsive noise and AWGN. The results obtained showed that good performances are achieved. However, it was the perfect case. The reality of power substations considers multipath components due to the presence of metallic structures, equipment, and devices. In order to take into account the aforementioned aspects, we now consider a deterministic channel extracted from the RapSor software [12]. Our objective is to acquire the channel impulse response (CIR) of the simulated channel matrix $[n_r \times n_t]$ coefficients. For this purpose, we select a HV substation located in Quebec (Canada) operated by the energy company Hydro-Quebec. Our WSN application consists of a 6×4 virtual MIMO system made up with the DGN node as the receiver placed on a tower of 60 m and the sensors forming a 10-node cluster mounted on transformers serving as the emitters. The clustering distance is approximately 14 m, while the long-haul distance is 1029 m.

6.2.1. Transmission without Node Selection. We consider the same situation as for the Rayleigh fading channel. However, only results for 4×4 MIMO are depicted, since they achieve the best performance. The results obtained are plotted in Figure 8. For the uncoded system, we notice a performance degradation when the channel is affected by impulsive noise. As for Rayleigh channel, a flattening of the BER curve

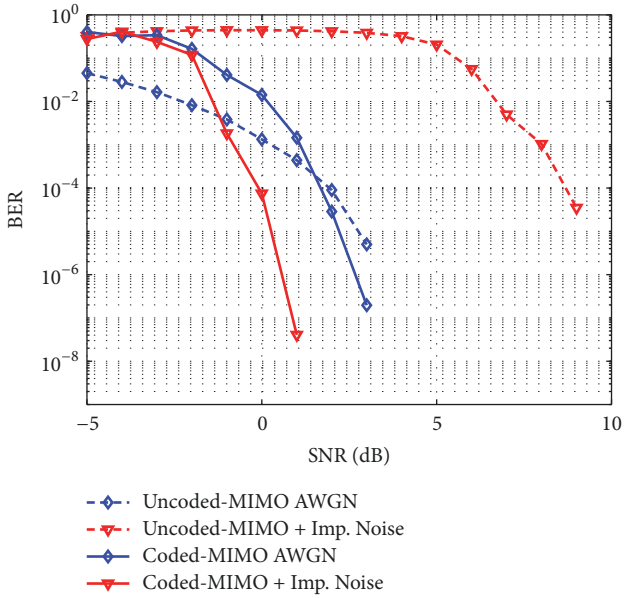

FIGURE 8: BER performance for max – d_{min} MIMO precoding with FCSI under RapSor channel without node selection.

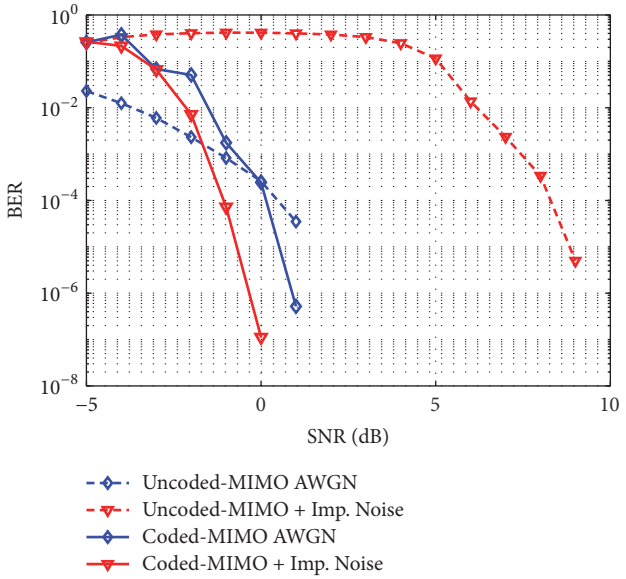

FIGURE 9: BER performance for max – d_{min} MIMO precoding with FCSI under RapSor channel with node selection.

between -3 and 2 dB can be noticed in the presence of impulsive noise. However, by combining the concatenated codes and max – d_{min} precoder with MIMO, we have an increase of system performance. Target BER of 10^{-4} is achieved at SNR of 0 and 8.7 dB for coded and uncoded MIMO, respectively, when the channel is affected by impulsive noise. It yields to a coding gain of 8.7 dB between uncoded and coded MIMO systems.

6.2.2. Transmission with Node Selection. In this section, optimal node selection is implemented to select 2 and 4 transmit nodes from the cluster of 10. Assuming the full channel knowledge, we explore the BER results for both coded and uncoded MIMO systems. The results are depicted in Figure 9. For the uncoded case, we can note the degradation of the performance. This is improved when the concatenation of codes is added. Target BER of 10^{-4} is achieved at SNR = -1 dB for coded MIMO, while it is 8 dB for uncoded system, when the channel is affected by impulsive noise.

7. Energy Consumption

7.1. Energy Model. The max – d_{min} protocol employs cooperative MIMO with the distributed nodes serving as multiple antennas. Hence, we are concerned with the total energy consumption E_{coop} of the nodes for a complete communication. According to the protocol description, the total energy of the cooperating nodes can now be expressed as

$$E_{coop} = E_{loc} + E_{init} + E_{fbk} + E_{MIMO} \tag{30}$$

where E_{loc} is the local transmission energy, i.e., the SISO communication between the nodes, E_{init} is the initialization phase, E_{fbk} is the feedback control channel energy, and E_{MIMO} is the energy of the data packet for MIMO transmission.

The average energy consumption of a radio frequency (RF) system can broadly be separated into P_{Amp} and P_{cct} which are the power consumption of power amplifiers and other circuits blocks, respectively. The model of typical RF blocks [30] representing the emitter is depicted in Figure 10, while the receiver can be seen in Figure 11.

The P_{Amp} is expressed as

$$P_{Amp} = \frac{\varsigma}{\varepsilon} P_{out} = \frac{\varsigma}{\varepsilon} \frac{E_b}{N_0} \frac{(2\pi)^2 d^{L_0} L_m D_r}{A g_t A g_r \lambda^2} R_b \tag{31}$$

ς is the peak-to-average ratio (PAR), ε corresponds to the power amplifier efficiency, E_b/N_0 is the ratio energy per bit to the noise, Ag_t and Ag_r are the emitter and the receiver antenna gains, respectively, L_m is the margin component which compensates for the variations of the hardware process and other noises, λ is the wavelength, D_r is the power density at the receiver, d is the long-haul distance, L_0 is the path-loss component, and R_b is the bit rate. The total power dissipated in circuit, P_{cct} for n_t transmitters and n_r receivers can be approximately expressed as

$$\begin{aligned} P_{cct} &= \left(P_{DAC} + P_{filt} + P_{mix} + P_{synth}\right) \\ &\quad + \left(P_{filr} + P_{LNA} + P_{mix} + P_{IFA} + P_{ADC}\right) \\ &= n_t P_c^{T_x} + n_r P_c^{R_x} \end{aligned} \tag{32}$$

where P_{DAC} and P_{ADC} are consumed energy for the digital-to-analogue converter (DAC) and the analogue-to-digital converter (ADC), respectively. P_{filt}t is the power consumed for the active filters at the transmitter, whereas P_{mix} and P_{filr} are the energy consumed for the mixer and the active

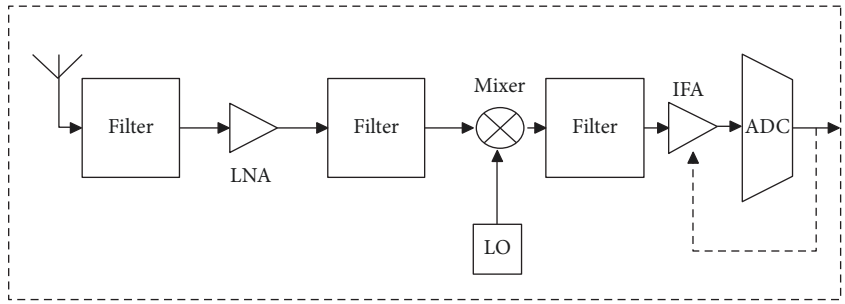

Figure 10: Transmitter circuit block.

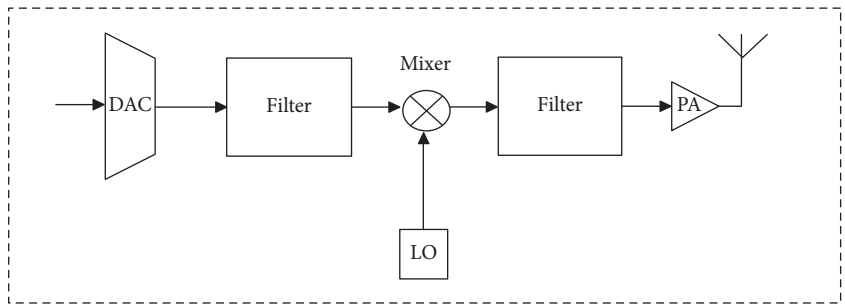

Figure 11: Receiver circuit block.

filters at the receiver, respectively. P_{LNA}, P_{synth}, and P_{IFA} are the power consumption for the Low-Noise Amplifier (LNA), the frequency synthesizer, and the Intermediate Frequency Amplifier, respectively. Parameters $P_c^{T_x}$ represent power dissipated in the circuit for a single node during data transmission and $P_c^{R_x}$ for reception. Total energy consumed per bit, E_{bit}, for a fixed-rate system is evaluated in the following equation:

$$E_{bit} = \frac{P_{Amp} + P_{cct}}{R_b} \tag{33}$$

Assuming a packet size of D symbols is to be transmitted and training symbols size of pn_t is inserted (p symbols are transmitted by each node), the effective bit rate R_b^{eff} is

$$R_b^{eff} = \left(\frac{D - pn_t}{D}\right) R_b \tag{34}$$

Note that replacing R_b in equation (31) by R_b^{eff}, we obtained the energy consumption model which accounts for the supplementary energy due to the p training symbols. For the max $- d_{min}$ MIMO precoding transmission, the bit rate R_b can, thus, be calculated as follows:

$$R_b = RmB \tag{35}$$

where R is the MIMO transmission rate, expressed as a ratio of the number of symbols transmitted, N_S, over the number of periods, N_P (i.e., $R = N_S/N_P$). $m = \log_2(M)$, where M is the constellation size, and B is the modulation bandwidth. Parameter E_{loc} is the total local transmission energy expended within a cluster k that consists of n_c nodes, separated by an average distance of d_c. Each source node can transmit to $n_r = (n_c - 1)$ receivers; thus, E_{loc} is expressed as

$$E_{loc} = N_{pkt}\left(\frac{P_{Amp} + P_{cct}}{R_b^{eff}}\right) \quad with\ P_{cct} = P_c^{T_{xk}} + (n_c - 1) P_c^{R_{xk}} \tag{36}$$

where $N_{pkt} = n_c L$ is the total number of bits in all sent packets, and for the random nodes cooperative transmission scenario, $n_c = n_t$. In (37), the training phase energy, E_{init} is given, where N_{T_S} is the amount of training bits

$$E_{init} = N_{T_S}\left(\frac{P_{Amp} + P_{cct}}{R_b^{OSTBC}}\right) \quad with\ P_{cct} = (n_c) P_c^{T_{xk}} \tag{37}$$

Only Alamouti's code yields a rate, $R = 1$, for complex modulations. The OSTBC solution for any value of n_t, but with $R = 1/2$ is presented in [31]. Solutions for $n_t = 3$ and 4, but with $R = 3/4$ are similarly presented. To implement our training phase for 10 (n_c) cluster nodes, we consider 4 × 4 OSTBC transmission. Then, we average rate to obtain $R_b^{OSTBC} = 2/3$ and the E_b/N_0 at the target BER. On the feedback channel, the energy E_{fbk} consumed is

$$E_{fbk} = \left(N_{fbk}\frac{n_t P_c^{R_{xk}}}{R_b}\right) \tag{38}$$

where n_t sensor nodes act as receivers; in this case, N_{fbk} is the number of bits sent on the feedback channel. The values of 3, 5, and 7 bits are considered for N_{fbk} when 2, 3, and 4 nodes are selected, respectively. Note that max $- d_{min}$ based selection requires $\lceil \log_2 L \rceil$ bits which have been included in N_{fbk}, where $\lceil \bullet \rceil$ denotes the nearest higher integer. Energy

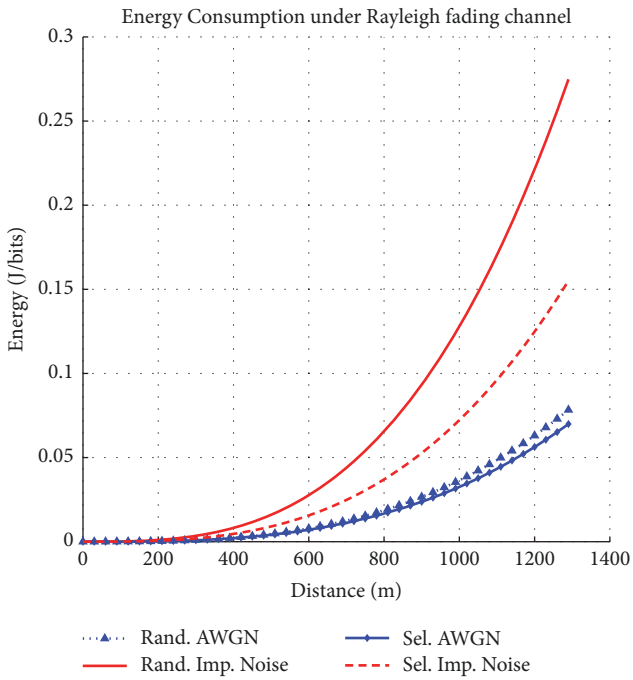

FIGURE 12: Energy consumption for max $-d_{min}$ precoding with FCSI under Rayleigh fading channel.

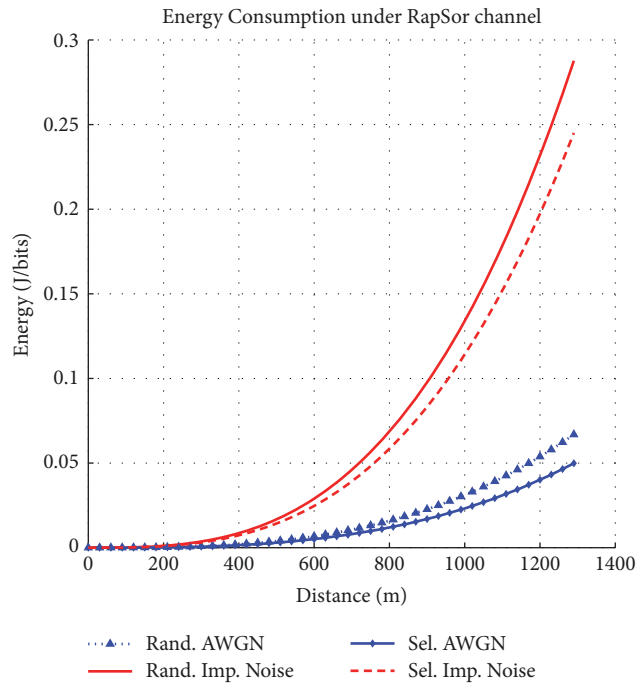

FIGURE 13: Energy consumption for max $-d_{min}$ precoding with FCSI under RapSor channel.

TABLE 1: Nodes and PAR parameters for energy computation.

Parameters	Values
Gains	2.5 dBi
Frequency carrier	2.5 GHz
Bandwidth	20 MHz
Power Amp. efficiency	0.35
BER	10^{-4}

required for the transmission of the data packets by MIMO technique using the max $- d_{min}$ precoder is

$$E_{MIMO} = N_{pkt}\left(\frac{P_{Amp} + P_{cct}}{R_b^{eff-prec}}\right) \quad (39)$$

$R_b^{(\bullet)}$ is the efficiency of the MIMO technique used in transmitting the symbols over b subchannels. Hence, $R_b^{eff-prec} = 2$.

7.2. Energy Consumption Evaluation. This section analyzes simulation results for energy consumption according to equation (30). The parameters used to compute the simulations are provided in Table 1.

We compute the total consumed energy for 4×4 MIMO systems. Figure 12 compares the consumed energy with and without selecting nodes for transmission. The AWGN and impulsive noise are considered in a Rayleigh fading channel.

As can be seen in this figure, the node selection technique reduces the total consumed energy. The energy is reduced from 0.27 to 0.16 J/bits corresponding to about 40% when the channel is corrupted by impulsive noise and the node selection is applied. However, we notice that the nodes require more energy to transmit to the DGN at the target BER, when the channel is affected by impulsive noise compared to the classical Gaussian noise.

Finally, Figure 13 shows the energy consumption per bit in a RapSor channel affected by AWGN and impulsive noise. As for the BER, only the results for 4 cooperative nodes are presented.

Similarly, for a Rayleigh channel, the energy is also reduced by 18%, that is, from 0.29 to 0.24 J/bits.

8. Conclusion

Linear precoders optimize a particular criterion using channel knowledge. They are based on the SVD to diagonalize the channel. Among these precoders, the max $- d_{min}$ precoder maximizes the minimum distance of the constellation in reception. It presents a maximal order of diversity $n_t \times n_r$. Based on the benefits of these techniques, we have proposed a reliable and efficient communication system by combining a concatenated RC with CC scheme and MIMO using max $- d_{min}$ precoder. We have also reduced the energy transmission with an efficient node selection technique in impulsive noise environment. With BPSK modulation over Rayleigh fading channel and deterministic ray tracing RapSor channel, we have explored the performance of the suggested proposal. The concatenation of max $- d_{min}$ and RC/CC leads to a large performance improvement. The SNR at the target BER reduces as the spatial diversity of MIMO system increases. Notice that the use of rank metric code also improves the reliability of the system compared to the uncoded case. FCSI is more useful than QCSI as can be observed in the results. Globally, the obtained results clearly demonstrate that the

max – d_{min} with FCSI and RC code are suitable for the impulsive noise mitigation.

We also investigate the energy efficiency for the node selection algorithm. To evaluate the robustness of the node selection technique, we use MIMO transmissions in communication channel impaired by noises. The disrupted noise was implemented using Au model validated by measurements. Results show that the node selection technique can achieve a maximum average amount of 40% in energy saving for 4 selected nodes in Rayleigh fading channels. However, the energy saving is about 18% in RapSor channel. In conclusion, as for the BER, this technique minimizes the energy consumption in both Rayleigh and realistic RapSor channels.

Data Availability

The data used to support the findings of this study are available from the corresponding author upon request.

Conflicts of Interest

The authors declare no conflicts of interest regarding the publication of this paper.

Acknowledgments

The authors would like to thank Dr. Minh Au at Hydro-Quebec Research Institute (IREQ), Canada, for the impulsive noise measurements, and Abdul Karim Yazbeck Ph.D. student at XLIM Institute, Limoges, France, for his work on the channel coding. The work in this paper is supported partially by grants from the Richard J. Marceau Research chair on Wireless IP technology for Developing Countries, partially by Institut de Recherche d'Hydro-Québec (IREQ), and partially by Labex ∑-Lim.

References

[1] P. P. Parikh, M. G. Kanabar, and T. S. Sidhu, "Opportunities and challenges of wireless communication technologies for smart grid applications," in *Proceedings of the IEEE Power and Energy Society General Meeting*, 2010.

[2] F. Sacuto, F. Labeau, J. Beland et al., "Impulsive noise measurement in power substations for channel modeling in ISM band," in *Proceedings of the CIGRE Canada Conference*, September 2012.

[3] M. Vu and A. Paulraj, "Some asymptotic capacity results for MIMO wireless with and without channel knowledge at the transmitter," in *Proceedings of the Conference Record of the Thirty-Seventh Asilomar Conference on Signals, Systems and Computers*, pp. 258–262, USA, November 2003.

[4] M. Vu and A. Paulraj, "Optimal linear precoders for MIMO wireless correlated channels with nonzero mean in space-time coded systems," *IEEE Transactions on Signal Processing*, vol. 54, no. 6 I, pp. 2318–2332, 2006.

[5] C. Tepedelenlioğlu and P. Gao, "On diversity reception over fading channels with impulsive noise," *IEEE Transactions on Vehicular Technology*, vol. 54, no. 6, pp. 2037–2047, 2005.

[6] S. Al-Dharrab and M. Uysal, "Cooperative diversity in the presence of impulsive noise," *IEEE Transactions on Wireless Communications*, vol. 8, no. 9, pp. 4730–4739, 2009.

[7] O. J. Oyedapo, B. Vrigneau, R. Vauzelle, and H. Boeglen, "Performance analysis of closed-loop MIMO precoder based on the probability of minimum distance," *IEEE Transactions on Wireless Communications*, vol. 14, no. 4, pp. 1849–1857, 2015.

[8] T. Nguyen, O. Berder, and O. Sentieys, "Cooperative MIMO schemes optimal selection for wireless sensor networks," in *Proceedings of the 2007 IEEE 65th Vehicular Technology Conference*, pp. 85–89, Dublin, Ireland, April 2007.

[9] N. Mysore, *Turbo-Coded MIMO Systems: Receiver Design and Performance Analysis [Ph.D. thesis]*, McGill University, 2006.

[10] Y. Li and M. Salehi, "Coded MIMO systems with modulation diversity for block-fading channels," in *Proceedings of the 2012 46th Annual Conference on Information Sciences and Systems (CISS)*, September 2012.

[11] N. B. Sarr, A. K. Yazbek, H. Boeglen, J. Cances, R. Vauzelle, and F. Gagnon, "An impulsive noise resistant physical layer for smart grid communications," in *Proceedings of the ICC 2017 - 2017 IEEE International Conference on Communications*, pp. 1–7, Paris, France, May 2017.

[12] C. Lièbe, P. Combeau, A. Gaugue et al., "Ultra-wideband indoor channel modelling using ray-tracing software for through-the-wall imaging radar," *International Journal of Antennas and Propagation*, vol. 2010, Article ID 934602, 14 pages, 2010.

[13] M. Au, F. Gagnon, and B. L. Agba, "An experimental characterization of substation impulsive noise for a RF channel model," in *Proceedings of the Progress in Electromagnetics Research Symposium, PIERS 2013 Stockholm*, vol. 1, pp. 1371–1376, Sweden, August 2013.

[14] P. Delsarte, "Bilinear forms over a finite field, with applications to coding theory," *Journal of Combinatorial Theory, Series A*, vol. 25, no. 4, pp. 226–241, 1978.

[15] A. Spaulding and D Middleton, "Optimum reception in an impulsive interference environment-part 1: coherent detection," *IEEE Transactions on Communications*, vol. 25, no. 9, pp. 910–923, 1977.

[16] G. A. Tsihrintzis and C. L. Nikias, "Fast estimation of the parameters of alpha-stable impulsive interference," *IEEE Transactions on Signal Processing*, vol. 44, no. 6, pp. 1492–1503, 1996.

[17] F. Sacuto, F. Labeau, and B. L. Agba, "Wide band time-correlated model for wireless communications under impulsive noise within power substation," *IEEE Transactions on Wireless Communications*, vol. 13, no. 3, pp. 1449–1461, 2014.

[18] N. B. Sarr, H. Boeglen, B. L. Agba, F. Gagnon, and R. Vauzelle, "Partial discharge impulsive noise in 735 kV electricity substations and its impacts on 2.4 GHz ZigBee communications," in *Proceedings of the 2016 International Conference on Selected Topics in Mobile and Wireless Networking, MoWNeT 2016*, Egypt, April 2016.

[19] E. E. M. Gabidulin, "Theory of codes with maximum rank distance," *Problemy Peredach Informatsii*, vol. 21, no. 1, pp. 3–16, 1985.

[20] A. W. Kabore, V. Meghdadi, J. Cances, P. Gaborit, and O. Ruatta, "Performance of Gabidulin codes for narrowband PLC smart grid networks," in *Proceedings of the 2015 International Symposium on Power Line Communications and its Applications (ISPLC)*, pp. 262–267, Austin, TX, USA, March 2015.

[21] E. M. Gabidulin, "Rank-metric codes and applications," http://iitp.ru/upload/content/839/Gabidulin.pdf.

[22] S. Plass, G. Richter, and A. J. Han Vinck, *Coding Schemes for Crisscross Error Patterns*, Springer Science+Business Media, LLC, 2007.

[23] P. Stoica and G. A. Ganesan, "Maximum-SNR spatial-temporal formatting designs for MIMO channels," *IEEE Transactions on Signal Processing*, vol. 50, no. 12, pp. 3036–3042, 2002.

[24] L. Collin, O. Berder, P. Rostaing, and G. Burel, "Optimal minimum distance-based precoder for MIMO spatial multiplexing systems," *IEEE Transactions on Signal Processing*, vol. 52, no. 3, pp. 617–627, 2004.

[25] D. J. Love, R. W. Heath Jr., V. K. N. Lau, D. Gesbert, B. D. Rao, and M. Andrews, "An overview of limited feedback in wireless communication systems," *IEEE Journal on Selected Areas in Communications*, vol. 26, no. 8, pp. 1341–1365, 2008.

[26] D. J. Love and J. Heath, "Limited feedback unitary precoding for spatial multiplexing systems," *Institute of Electrical and Electronics Engineers Transactions on Information Theory*, vol. 51, no. 8, pp. 2967–2976, 2005.

[27] A. Goldsmith, *Wireless Communications*, Cambridge University Press, 2005.

[28] A. Charrada, "Nonlinear complex M-SVR for LTE MIMO-OFDM channel with impulsive noise," in *Proceedings of the 2016 7th International Conference on Sciences of Electronics, Technologies of Information and Telecommunications (SETIT)*, pp. 10–13, Hammamet, Tunisia, December 2016.

[29] G. A. Hussain, M. B. Mokhtar, and R. S. A. B. Raja, "Concatenated RS-convolutional codes for MIMO-OFDM system," *Asian Journal of Applied Sciences*, vol. 4, no. 7, pp. 720–727, 2011.

[30] S. Cui, A. J. Goldsmith, and A. Bahai, "Energy-efficiency of MIMO and cooperative MIMO techniques in sensor networks," *IEEE Journal on Selected Areas in Communications*, vol. 22, no. 6, pp. 1089–1098, 2004.

[31] V. Tarokh, H. Jafarkhani, and A. R. Calderbank, "Space-time block codes from orthogonal designs," *IEEE Transactions on Information Theory*, vol. 45, no. 5, pp. 1456–1467, 1999.